Lentiviral delivery of human erythropoietin attenuates hippocampal atrophy and improves cognition in the R6/2 mouse model of Huntington's disease

Neurobiology of Disease 144 (2020) 105024

Contents lists available at ScienceDirect

Neurobiology of Disease

journal homepage: www.elsevier.com/locate/ynbdi

Lentiviral delivery of human erythropoietin attenuates hippocampal atrophy and improves cognition in the R6/2 mouse model of Huntington's disease

Simone Rolfes[a], David A.D. Munro[b], Ekaterini-Maria Lyras[a], Eduardo Matute[a], Koliane Ouk[a,d], Christoph Harms[c], Chotima Böttcher[a,1], Josef Priller[a,b,d,*,1]

[a] Department of Neuropsychiatry and Laboratory of Molecular Psychiatry, Charité –Universitätsmedizin Berlin, 10117 Berlin, Germany
[b] UK Dementia Research Institute at the University of Edinburgh, Edinburgh EH16 4SA, UK
[c] Department of Experimental Neurology and Center for Stroke Research, Charité –Universitätsmedizin Berlin, 10117 Berlin, Germany
[d] DZNE Berlin, 10117 Berlin, Germany

ARTICLE INFO

Keywords:
Huntington's disease
Intracerebroventricular
Gene delivery
Transgenic mice
Therapy
Neurodegeneration

ABSTRACT

Huntington's disease (HD) is an incurable neurodegenerative disorder caused by a trinucleotide (CAG) repeat expansion in the huntingtin gene (*HTT*). The R6/2 transgenic mouse model of HD expresses exon 1 of the human *HTT* gene with approximately 150 CAG repeats. R6/2 mice develop progressive behavioural abnormalities, impaired neurogenesis, and atrophy of several brain regions. In recent years, erythropoietin (EPO) has been shown to confer neuroprotection and enhance neurogenesis, rendering it a promising molecule to attenuate HD symptoms. In this study, the therapeutic potential of EPO was evaluated in female R6/2 transgenic mice. A single bilateral injection of a lentivirus encoding human EPO (LV-hEPO) was performed into the lateral ventricles of R6/2 mice at disease onset (8 weeks of age). Control groups were either untreated or injected with a lentivirus encoding green fluorescent protein (LV-GFP). Thirty days after virus administration, hEPO mRNA and protein were present in injected R6/2 brains. Compared to control R6/2 mice, LV-hEPO-treated R6/2 mice exhibited reduced hippocampal atrophy, increased neuroblast branching towards the dentate granular cell layer, and improved spatial cognition. Our results suggest that LV-hEPO administration may be a promising strategy to reduce cognitive impairment in HD.

1. Introduction

Huntington's disease (HD) is a progressive neurodegenerative disorder caused by an abnormal CAG expansion in the huntingtin (*HTT*) gene (Huntington's Disease Collaborative Research Group, 1993). In HD, the mutant form of huntingtin (mHTT) is expressed in both the nervous system and peripheral tissues, but most clinical features of the disease can be attributed to degeneration in the central nervous system (CNS). Hallmarks of HD include the aggregation of mHTT in intracellular inclusions and the loss of medium spiny neurons in the striatum (DiFiglia et al., 1997). As the disease progresses, neuronal cell death also affects other brain regions, such as the hippocampus (Spargo et al., 1993). This neurodegeneration results in progressive brain atrophy (Bradford et al., 2009; Ross and Tabrizi, 2011) and a triad of motor, psychiatric and cognitive disturbances (Bates et al., 2015).

Mouse models have been developed to study disease mechanisms and to evaluate potential therapies for HD. The most widely used model is the R6/2 transgenic mouse line: these mice ubiquitously express exon 1 of the mutant human *HTT* gene with approximately 150 CAG repeats (Mangiarini et al., 1996). R6/2 mice recapitulate many features of human HD pathology, such as weight loss, decreased brain volume, reduced hippocampal neurogenesis, and progressive motor, cognitive and behavioural abnormalities (Stack et al., 2005; Phillips et al., 2005). Moreover, R6/2 mice develop deficits in spatial learning, a process that is associated with dendrite length and density in the hippocampus (Murphy et al., 2000; Bulley et al., 2012). Although several studies have proposed promising therapeutic strategies in R6/2 mice using, for example, environmental enrichment and pharmaceutical substances (Hockly et al., 2002; Schiefer et al., 2002; Stack et al., 2006; Peng et al., 2008; Squitieri et al., 2015; Ellrichmann et al., 2017), no curative therapies for HD are available.

In the adult CNS, the cytokine erythropoietin (EPO) is involved in

* Corresponding author at: Department of Neuropsychiatry and Laboratory of Molecular Psychiatry, Charité – Universitätsmedizin Berlin, Charitéplatz 1, 10117 Berlin, Germany.
E-mail address: josef.priller@charite.de (J. Priller).
[1] Both authors contributed equally.

https://doi.org/10.1016/j.nbd.2020.105024
Received 3 March 2020; Received in revised form 4 July 2020; Accepted 16 July 2020
Available online 20 July 2020

maintaining neuronal survival and cell proliferation (Digicaylioglu et al., 1995; Shingo et al., 2001; Chen et al., 2007). The application of recombinant human EPO (hEPO) has been shown to improve learning and memory in rodent models of depression, cerebral ischemia, and traumatic brain injury (Lu et al., 2005; Zhang et al., 2007; Girgenti et al., 2009; Leconte et al., 2011), and hEPO attenuates disease progression in a mouse model of amyotrophic lateral sclerosis (Grunfeld et al., 2007). In humans, the neurotrophic properties of EPO on cognitive function are also evident in diseases such as schizophrenia and multiple sclerosis (Ehrenreich et al., 2007; Wüstenberg et al., 2011).

The beneficial effects of recombinant hEPO are mediated through induction of anti-apoptotic, anti-oxidant, and anti-inflammatory signals and the promotion of neurite outgrowth, neurogenesis, and angiogenesis (Genc et al., 2002; Wen et al., 2002; Kumral et al., 2005; Oh et al., 2012). However, large amounts and multiple doses of peripherally administered recombinant hEPO are required to achieve a substantial therapeutic effect in the CNS parenchyma (Ehrenreich et al., 2004), which in turn can result in hematocrit-associated systemic side effects such as thrombosis and stroke (Patel et al., 2012). Intraperitoneal administration of the non-hematopoietic EPO metabolite, asialoerythropoietin, which has a very short half-life, failed to exert beneficial effects in R6/2 mice (Gil et al., 2004). To overcome the limitations discussed above, long-term CNS-restricted administration of EPO could alternatively be achieved using a gene transfer system such as lentiviral vectors. Lentiviral vectors are a robust tool for efficient gene transfer into the CNS due to their ability to transduce non-dividing and slowly dividing cells (Kantor et al., 2014). Lentiviral vectors can transduce most CNS cell types, including neurons, astroglia, and oligodendroglia (Blömer et al., 1997; Jakobsson et al., 2003; McIver et al., 2005; Fassler et al., 2013).

In this study, the therapeutic potential of lentiviral vectors encoding for human EPO (LV-hEPO) was evaluated in the R6/2 mouse model of HD.

2. Results

2.1. Expression of hEPO and GFP in R6/2 brains thirty days after bilateral intracerebroventricular injection of lentiviral vectors

To investigate the effects of EPO expression on HD related-phenotypes in R6/2 mice, we generated a lentivirus (LV) encoding for human EPO (LV-hEPO) (Fig. 1A), which we injected bilaterally into the lateral ventricles of the brain (ICV) of 8-week-old female R6/2 mice. Control mice were injected with a lentivirus encoding the green fluorescent protein GFP (LV-GFP) or were untreated.

Thirty days post-injection, hEPO mRNA was detected in the hippocampus, cortex and striatum of R6/2 mice that received LV-hEPO, but not in R6/2 mice that received LV-GFP (Fig. 1B). GFP mRNA was detected in the brains of LV-GFP injected mice, but not in LV-hEPO-treated animals (Fig. 1C). The presence of the hEPO protein in the brains of LV-hEPO-treated R6/2 mice was confirmed with an enzyme-linked immunosorbent assay (ELISA; Fig. 1D) and by immunohistochemistry (Fig. 1E). hEPO immunoreactivity was observed bilaterally in the dentate gyrus and the pyramidal layer of the hippocampus of LV-hEPO-treated R6/2 mice (Fig. 1E) with expression in $NeuN^+$ neurons (data not shown). No hEPO protein was detected in control R6/2 mice that received LV-GFP (Figs. 1D,F). Hematocrit levels were unchanged in LV-hEPO-treated animals (Fig. 1G).

Taken together, these data show that a single bilateral ICV injection of a lentivirus encoding hEPO resulted in long-term production of hEPO mRNA and protein in R6/2 brains, without causing adverse hematopoietic consequences.

2.2. Intracerebroventricular LV-hEPO administration attenuates the cognitive impairment in R6/2 mice but does not improve weight loss or motor impairments

To investigate the effects of lentivirus-mediated hEPO expression on HD related-phenotypes in R6/2 mice, we first performed motor and cognitive testing (the experimental timeline is outlined in Fig. 2A). A total of 8 female wildtype (WT) and 36 female R6/2 mice were used for this part of the study (7 untreated, 14 LV-GFP-treated and 15 LV-hEPO-treated R6/2 mice). All mice were 8-weeks old at the beginning of the experiment.

Progressive weight loss is a prominent phenotype of R6/2 mice and is a useful readout reflecting disease progression (Gil et al., 2004; El-Akabawy et al., 2012). The three groups of R6/2 mice (untreated, LV-GFP-injected, and LV-hEPO-injected) progressively lost weight, while their wildtype (WT) littermates gained weight over the observation period of 30 days (Fig. 2B). The body weight of LV-hEPO-treated R6/2 mice did not differ from untreated or LV-GFP-treated R6/2 mice (Fig. 2B), suggesting that hEPO does not prevent weight loss in this model.

In addition to weight loss, R6/2 mice display motor abnormalities, such as dyskinetic movements, resting tremor, handling/stress-induced seizures, and locomotor abnormalities (Mangiarini et al., 1996; Carter et al., 1999). We used the rotarod performance test to measure the effects of LV-hEPO administration on forelimb and hindlimb motor coordination at baseline (one day before injection, or experimental day −1), 11 days post-injection, and 28 days post-injection. All R6/2 mice (untreated, LV-GFP-injected, and LV-hEPO-injected) showed deficits in motor performance compared to WT littermates (Fig. 2C). LV-hEPO treatment of R6/2 mice did not attenuate the progressive deterioration of motor performance compared to untreated and LV-GFP-treated R6/2 mice (Fig. 2C).

Previous studies reported hypoactivity and decreased motor activity in R6/2 mice as determined by open field testing (Li et al., 2005). Therefore, we next used the open field test to measure the effects of LV-hEPO administration on overall activity by comparing baseline with days 15 and 30 post-injection. All three groups of R6/2 mice (untreated, LV-GFP-injected, and LV-hEPO-injected) travelled significantly less distance in the open field than WT littermates and LV-hEPO administration did not improve overall activity in R6/2 mice (Fig. 2D).

Another pathological phenotype observed in R6/2 mice is impaired spatial cognition, which manifests prior to the onset of an overt motor phenotype (Murphy et al., 2000). To evaluate whether LV-hEPO administration alleviated impaired cognitive function in R6/2 mice, we tested spatial working memory by quantifying spontaneous alternation behaviour using a Y-maze task (Fig. 2E). The experimental mice exhibited a progressive loss of spatial memory from day 15 to day 30 post-injection (mixed-effects model, time-effect: $p = .0345$) and the treatment/genotype of the mice considerably influenced their spontaneous alternation scores (mixed-effects model, treatment/genotype-effect: $p < .0001$). Notably, LV-hEPO-treated R6/2 mice exhibited increased spontaneous alternations compared to untreated and LV-GFP-treated R6/2 mice at both 15 and 30 days post-injection, and spatial cognition was normalised to the levels of WT littermates (Fig. 2F).

These data suggest that ICV LV-hEPO treatment specifically rescued the spatial cognition deficits in R6/2 mice, whereas weight loss and motor performance deficits were not improved.

2.3. Intracerebroventricular LV-hEPO administration reduces hippocampal atrophy in R6/2 mice without causing neuroinflammation

We next asked whether the improved spatial cognition observed after bilateral ICV injection of LV-hEPO in R6/2 mice may reflect disease modification. To test this, we performed a new experiment with a total of 6 female WT mice and 17 R6/2 mice (5 untreated, 6 LV-GFP-treated, and 6 LV-hEPO-treated R6/2 mice) to monitor the progression

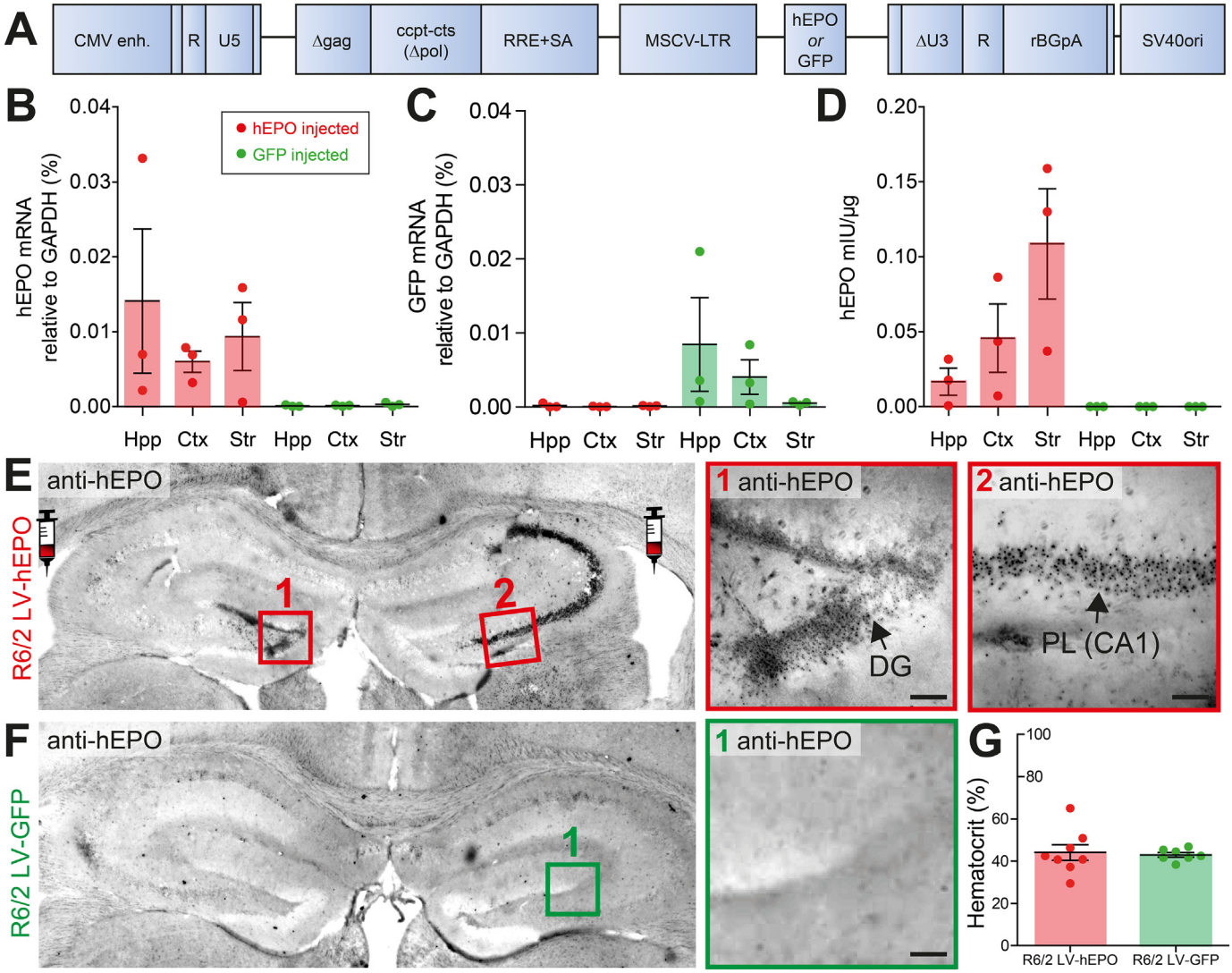

Fig. 1. Analysis of hEPO and GFP expression 30 days after lentiviral delivery. (**A**) Schematic of the HIV-1-based vector used in this study (pCL20c-MSCV; Hanawa et al., 2002). Eight-week-old female R6/2 mice received a bilateral injection of the lentivirus encoding hEPO or GFP into the lateral ventricles. The lentiviral vectors expressed hEPO or GFP under the control of the murine stem cell (MSCV) promoter. LTR, long terminal repeat; cPPt, central polpurine tract; CTS, central termination sequence; RRE, Rev-responsive element; rBGpA, rabbit ß-globin gene polyadenylation site; SV40ori, SV40 origin of replication. (**B**–**C**) qRT-PCR detection of (**B**) hEPO mRNA and (**C**) GFP mRNA in the hippocampus (Hpp), cortex (Ctx) and striatum (Str) of LV-hEPO and LV-GFP-treated R6/2 brains. Values are means ± SEM (n = 3 per group). (**D**) hEPO levels as determined by ELISA in the hippocampus, cortex, and striatum of R6/2 mice treated with LV-hEPO and LV-GFP. Data are means ± SEM (n = 3 per group). (***E***-**F**) Representative bright-field images showing immunohistochemical detection of hEPO protein in (**E**) LV-hEPO-treated R6/2 mice but not in (**F**) LV-GFP-treated mice. Syringe cartoons in **E** represent injection sites. DG, dentate gyrus; PL (CA1), pyramidal layer (*Cornu Ammonis* area 1). Scale bar = 50 µm. (**G**) No difference in the hematocrit levels of R6/2 mice treated with LV-hEPO (n = 8) and LV-GFP (n = 7) (p = .78; unpaired two-tailed t-test).

of brain atrophy in different brain regions using T2-weighted magnetic resonance imaging (MRI). At baseline (one day before injection), we detected significant atrophy of the cortex, striatum, and hippocampus of LV-GFP-treated R6/2 mice compared to WT littermates (Figs. 3A-D). Tissue volumes of grey matter regions (cortex, striatum and hippocampus) decreased progressively in R6/2 mice over the observation period (Figs. 3A,C,D). In contrast, white matter atrophy in the corpus callosum remained constant (Fig. 3B). At 15 and 30 days after LV-hEPO injection, hippocampal atrophy was significantly reduced in LV-hEPO-treated R6/2 mice compared to control LV-GFP-treated R6/2 mice (Fig. 3D), whereas no differences in atrophy of the other grey matter regions were observed (Figs. 3A,C). These results suggest specific preservation of hippocampal tissue volume by ICV LV-hEPO administration in R6/2 mice.

Since injection of high titres of lentivirus into the rodent brain may be associated with an inflammatory response (Abordo-Adesida et al., 2005) and microglia, the resident immune cells of the CNS, are activated in R6/2 mice (Simmons et al., 2018), we performed a new experiment to examine neuroinflammatory responses to ICV LV-hEPO administration in R6/2 mice (n = 7 WT, n = 5 untreated R6/2 mice, n = 6 LV-GFP-treated R6/2 mice, and n = 8 LV-hEPO-treated R6/2 mice). At experimental day 30, no significant differences in the number of Iba1$^+$ brain macrophages/microglia were found between WT mice, untreated R6/2 mice, LV-GFP-treated R6/2 mice, or LV-hEPO-treated R6/2 mice in the dentate gyrus (DG) of the hippocampus (Figs. 3E,F). We also did not detect statistically significant differences in hippocampal mRNA levels of the proinflammatory cytokines/chemokines, *tnf* (Fig. 3G) and *ccl2* (Fig. 3H), between the different groups of R6/2 mice. Consistent with these findings, flow cytometric analysis of hippocampal microglia isolated from WT, untreated R6/2, LV-GFP-treated R6/2, or LV-hEPO-treated R6/2 mice did not reveal statistically significant differences in the expression of TNFα or MHC class II molecules (Fig. 3I,J). Additionally, LV-hEPO treatment did not modify the tissue coverage by glial fibrillary acidic protein positive (GFAP$^+$) astrocytes in the

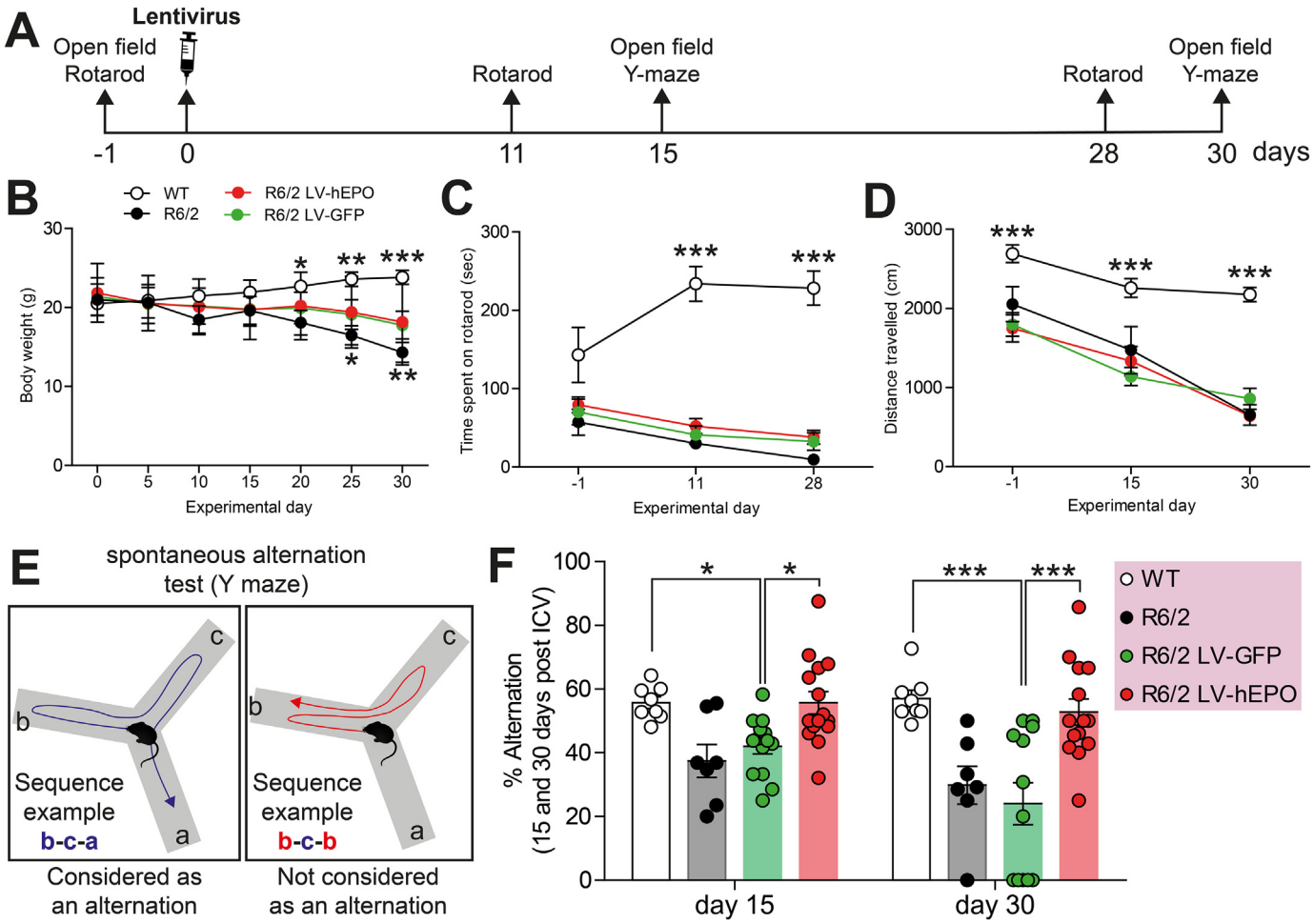

Fig. 2. Improved spatial cognition of LV-hEPO-treated R6/2 mice. (**A**) Schematic depicting the experimental pipeline. Four groups of female mice were tested (WT, n = 8; untreated R6/2 mice, n = 7; LV-GFP-treated R6/2 mice, $n = 14$; LV-hEPO-treated R6/2 mice, $n = 15$). (**B**) Body weight measurements over the experimental period. (**C**) Motor performance as determined using rotarod testing. (**D**) Exploratory activity was examined using the open field test. (**E**) Schematic describing alternations in the Y-maze test. A sequential triad of alternating arm entries is considered as an alternation. (**F**) Spatial cognition scores based on the percentage of alternations in the Y-maze test at 15 days and 30 days post-injection. Statistical tests used for **B-D** and **F** = Mixed-effects analysis with two-stage linear step-up procedure of Benjamini, Krieger and Yekutieli as post-tests by controlling the False Discovery Rate (individually comparing each group to each other group). For illustrative purposes, only statistically significant differences compared to the LV-GFP-treated R6/2 group are shown. $*p < .05$, $**p < .01$, $***p < .001$.

hippocampus, cortex or striatum of R6/2 mice (Fig. 4A-D). These data suggest that the lentiviral-mediated transgene expression did not provoke neuroinflammation or astrogliosis.

As mHTT progressively forms aggregates in the brains of R6/2 mice (Morozko et al., 2018), we next explored whether the lentiviral delivery of hEPO modified mHTT accumulation in this mouse model. As anticipated, mHTT aggregates (detected using an anti-huntingtin antibody [EM48]) were not observed in WT brains, but were present in R6/2 brains (Fig. 4A,B). Importantly, we did not detect significant differences in mHTT accumulation in the hippocampus, cortex, or striatum of LV-hEPO-treated R6/2 mice compared to LV-GFP-treated R6/2 mice (Fig. 4A-C, E). These results suggest that lentiviral delivery of hEPO does not modify mHTT aggregation in R6/2 mice.

2.4. Intracerebroventricular LV-hEPO administration enhances neurite branching in hippocampal neuroblasts but does not increase adult neurogenesis in R6/2 mice

We hypothesized that the normalization of spatial learning (Fig. 2) and reduction of hippocampal atrophy (Fig. 3) observed after ICV LV-hEPO injection in R6/2 mice may result from enhanced hippocampal neurogenesis. In agreement with previous reports showing impaired hippocampal neurogenesis in R6/2 mice (Gil et al., 2004; Phillips et al., 2005), we detected reduced numbers of doublecortin (DCX)-immunoreactive neuroblasts, and reduced numbers of proliferating bromodeoxyuridine (BrdU)-positive cells in the DG of all groups of R6/2 mice compared to WT mice at 30 days after BrdU-injection (Fig. 5A,B). Neither the administration of LV-GFP nor LV-hEPO rescued this phenotype (Fig. 5A,B). The percentage of proliferating neuroblasts (DCX^+BrdU^+) was not significantly different between the groups of mice (Fig. 5C). These results indicate that LV-hEPO administration did not improve adult neurogenesis in the hippocampus of R6/2 mice.

As EPO has been shown to increase neurite outgrowth in neural progenitor cells from the hippocampus (Oh et al., 2012) and subventricular zone (Wang et al., 2006), we examined neurite branching from DCX^+ neuroblasts in the dentate gyrus. We detected significantly increased neuroblast branching in LV-hEPO-treated R6/2 mice compared to control R6/2 mice (Fig. 5D,E). No significant differences in neuroblast migration were detected between the groups of mice (Fig. 5F).

Collectively, our data show that, as well as exhibiting reduced hippocampal atrophy and improved spatial cognition, neurite branching of neuroblasts was increased in LV-hEPO-treated R6/2 mice compared to untreated R6/2 mice (Fig. 5G).

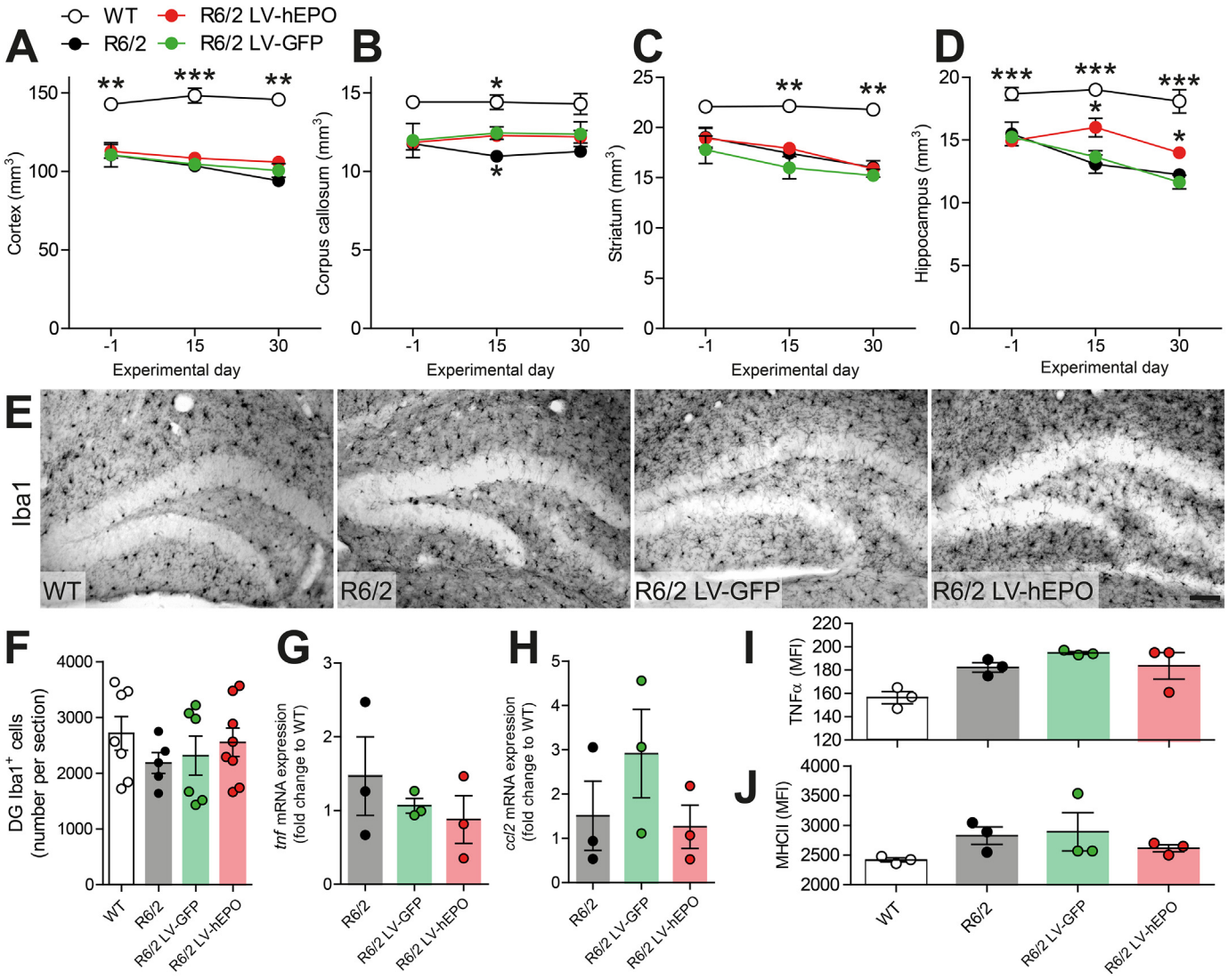

Fig. 3. Reduced hippocampal atrophy in LV-hEPO-treated R6/2 mice. (**A-D**) Volume changes in different brain regions over the experimental period of 30 days in four groups of tested mice. Day −1: WT, $n = 6$; untreated R6/2 mice, $n = 5$; R6/2 LV-GFP mice, n = 6; R6/2 LV-hEPO mice, $n = 6$. Day 15: WT, n = 6; untreated R6/2 mice, n = 5; R6/2 LV-GFP mice, $n = 4$; R6/2 LV-hEPO mice, $n = 5$. Day 30: WT, n = 6; untreated R6/2 mice, n = 5; R6/2 LV-GFP mice, n = 3; R6/2 LV-hEPO mice, $n = 4$. (**E**) Immunohistochemistry for Iba1 (brain macrophage/microglial marker) at experimental day 30. Representative images of the DG of WT mice (n = 7), untreated R6/2 mice (n = 5), R6/2 mice treated with LV-GFP (n = 6), and R6/2 mice treated with LV-hEPO (n = 8) are shown. (**F**) Microglial numbers in the dentate gyrus (DG) between the different groups of mice. (**G-H**) Expression of (**G**) *tnf* mRNA or (**H**) *ccl2* mRNA in the hippocampus of untreated, LV-GFP-treated, and LV-hEPO-treated R6/2 mice (n = 3 per group). (**I-J**) Expression of (**I**) TNFα and (**J**) MHC class II on microglia isolated from the hippocampus of the different groups of mice (n = 3 per group). MFI, mean fluorescence intensity. Statistical tests used for **A-D** = Mixed-effects analysis with two-stage linear step-up procedure of Benjamini, Krieger and Yekutieli as post-tests by controlling the False Discovery Rate (individually comparing each group to each other group). For illustrative purposes, only statistically significant differences compared to the LV-GFP-treated R6/2 group are shown. Test used for **F** = one-way ANOVA. Tests used for **G-J** = Kruskal-Wallis tests. *p < .05, **p < .01, ***p < .001. Scale bar = 100 μm.

3. Discussion

HD is an incurable monogenic disorder that results in the dysfunction and death of neurons, with disease onset typically in adulthood. Although numerous studies have demonstrated that EPO can act as a neuroprotective agent in various neurological diseases, few have investigated its therapeutic potential in HD. Here, we administered a single bilateral injection of LV-hEPO into R6/2 mouse brains and assessed the progression of HD-associated symptoms, finding that several hippocampus-related deficits were attenuated. Our results show that in vivo administration of LV-hEPO can exert protective effects in a HD mouse model, without adverse hematopoietic consequences.

Brain atrophy is a common symptom of HD (Bates et al., 2015). In this study, LV-hEPO-treated R6/2 mice exhibited increased neurite branching in the dentate gyrus and reduced hippocampal volume loss compared to control R6/2 mice. These findings are consistent with previous studies showing that EPO can stimulate expression of neurotrophic factors in the dentate gyrus (Girgenti et al., 2009; Sathyanesan et al., 2018), increase neurite outgrowth in cultures of dissociated hippocampal neurons (Oh et al., 2012), and protect against hippocampal atrophy in disease (Wüstenberg et al., 2011; Miskowiak et al., 2015). Mechanisms of hippocampal atrophy in disease are incompletely understood, but preclinical trials suggest that both dendritic retraction and neuronal cell death contribute (Hageman et al., 2008; Czéh and Lucassen, 2007). While we did not globally analyze dendrite retraction throughout the hippocampal formation, we demonstrate that dendrite branching was maintained in the dentate gyrus, suggesting a mechanism by which EPO may protect against hippocampal volume loss.

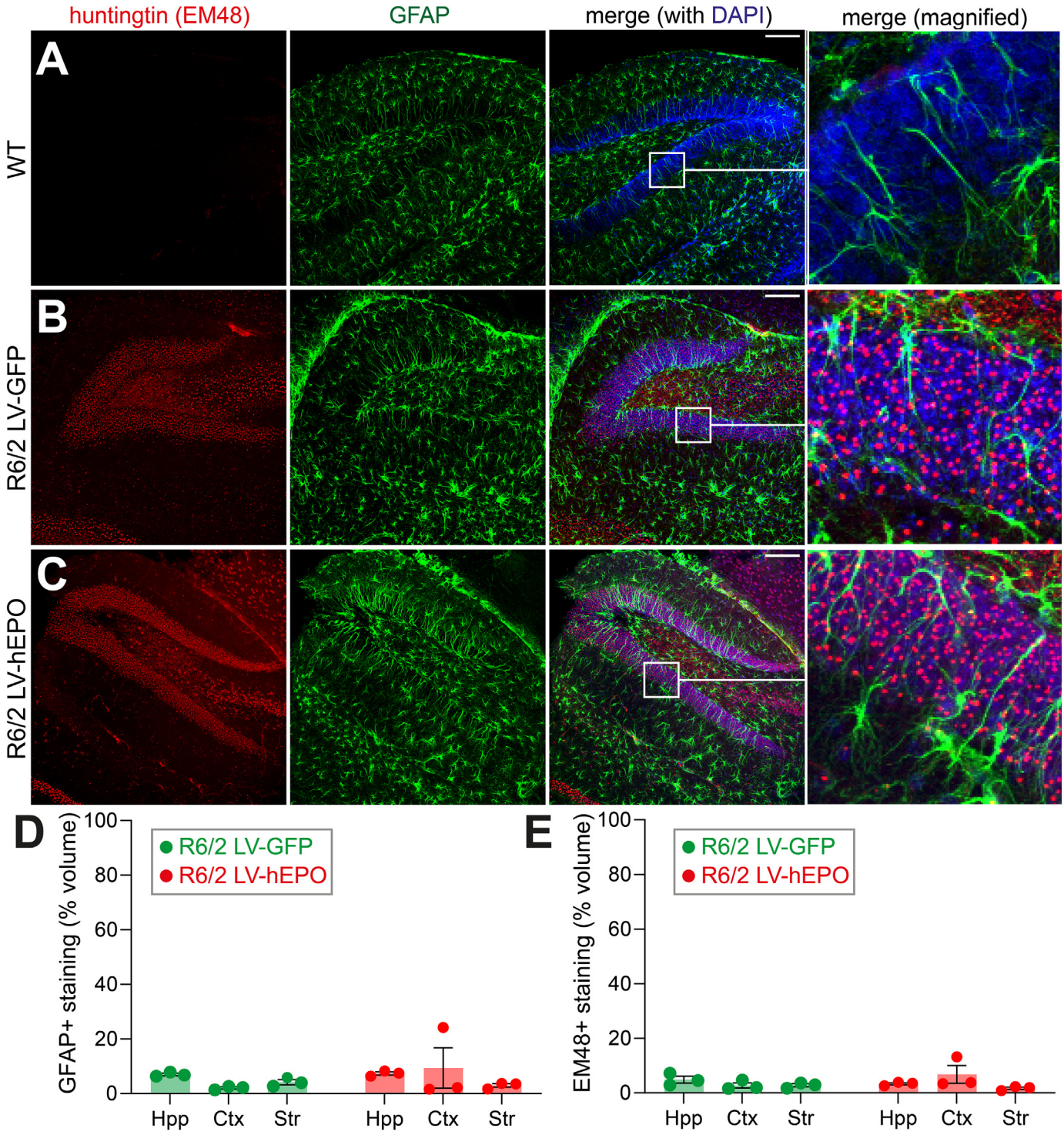

Fig. 4. LV-hEPO treatment does not modify astrocyte activation or mutant huntingtin aggregation in R6/2 mice. (**A-C**) Representative images showing EM48 immunoreactivity (red, mHTT aggregates) and GFAP immunoreactivity (green, astrocytes) in the dentate gyrus of (**A**) WT, (**B**) LV-GFP-treated, and (**C**) LV-hEPO-treated mice (representative of n = 3 mice per group). Nuclei were counterstained with DAPI (blue). (**D-E**) Quantification of volume covered by (**D**) GFAP immunoreactivity and (**E**) huntingtin immunoreactivity in the hippocampus (Hpp), cortex (Ctx), and striatum (Str) of LV-GFP-treated and LV-hEPO-treated R6/2 mice (n = 3 mice per group; 3 individual z-planes from each area were pooled for analysis per mouse). Data are means ± SEM. Groups did not differ significantly (Wilcoxon-Mann-Whitney tests). Scale bars = 100 µm. (For interpretation of the references to colour in this figure legend, the reader is referred to the web version of this article.)

We demonstrated that LV-hEPO-treated R6/2 mice exhibited improved spatial cognition compared to control R6/2 mice, which is in line with previous studies showing EPO-associated improvements in cognition (Ehrenreich et al., 2007; Al-Qahtani et al., 2014; Almaguer-Melian et al., 2015; Othman et al., 2018). Furthermore, EPO-treatment has been shown to enhance synaptic connectivity and long-term potentiation within the mouse hippocampus, as measured by neurophysiology on hippocampal slices (Adamcio et al., 2008). As neural networks within the hippocampus support spatial cognition (O'Keefe and Nadel, 1978; Schmidt-Hieber and Nolan, 2017), we speculate that the

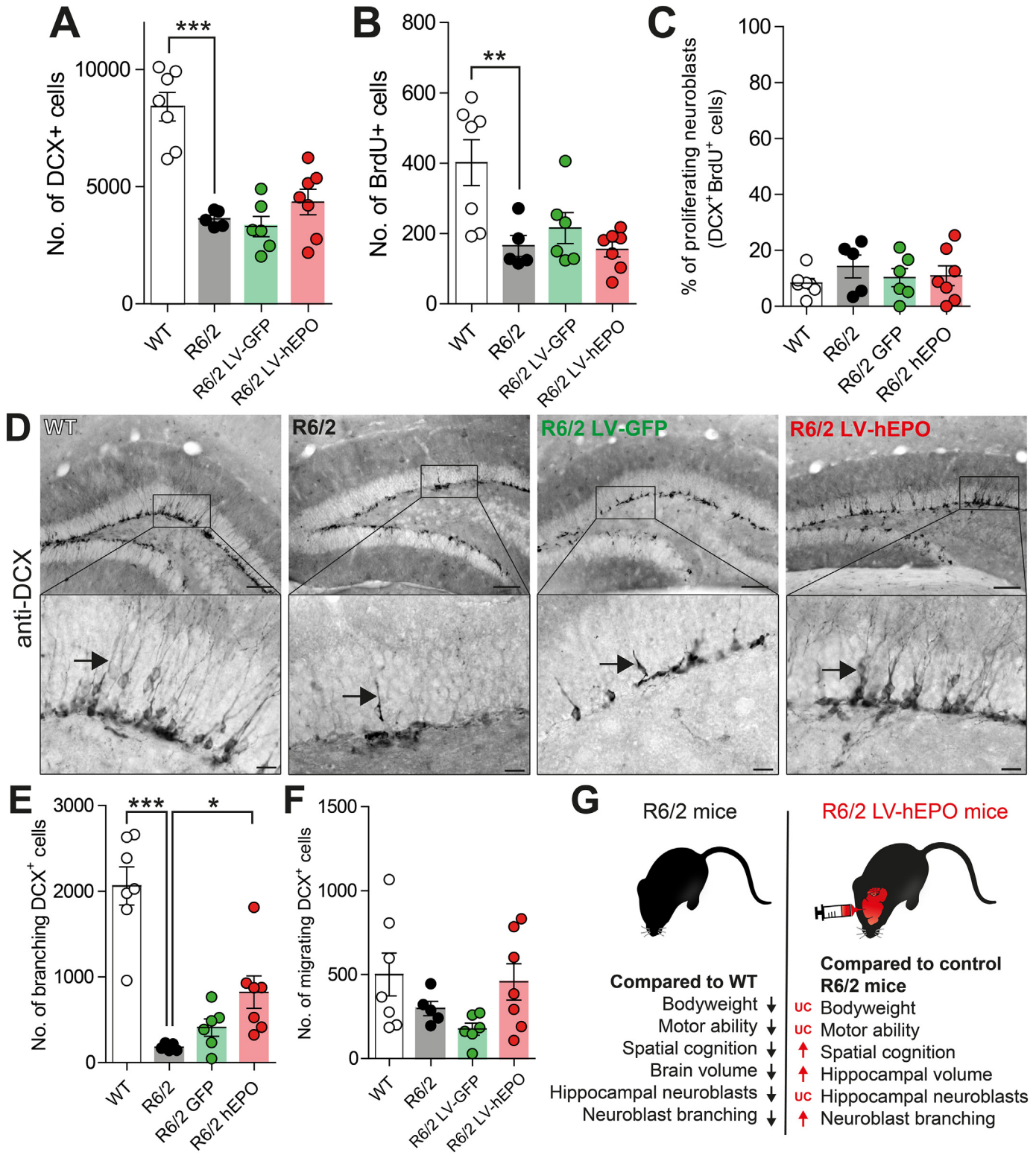

Fig. 5. Increased neuroblast branching in the dentate gyrus (DG) of LV-hEPO-treated R6/2 mice. (**A-C**) Immunohistochemical analysis of DG neurodegenesis. Number of (**A**) DCX^+ neuroblasts, (**B**) proliferating $Brdu^+$ cells, and (**C**) proliferating DCX^+BrdU^+ neuroblasts in the DG at 30 days after BrdU injection in WT mice (n = 7) and untreated (n = 5), LV-GFP-treated (n = 6) and LV-hEPO-treated (n = 7) R6/2 mice. (**D**) Representative images showing DCX^+ neuroblast branching (black arrows) in the DG of WT mice and untreated, LV-GFP-treated and LV-hEPO-treated R6/2 mice. (**E**) Number of branching DCX^+ neuroblasts. (**F**) Number of migrating DCX^+ neuroblasts in the hippocampus. (**G**) Overview of effects of LV-hEPO-treatment on R6/2 mice. UC, unchanged. Statistical tests used for **A-C** and **E-F** = one-way ANOVA with Dunnett's multiple comparison post-tests (individually comparing each group to the R6/2 group). *p < .05, **p < .01, ***p < .001. Scale bars = 100 μm for overview images and 20 μm for magnifications.

hippocampal preservation observed in the LV-hEPO-treated mice may have permitted the maintenance of spatial cognition in these animals.

A previous study similarly aimed to improve HD-related phenotypes in R6/2 mice without increasing hematocrit via intraperitoneal administration of asialoerythropoietin, an EPO variant that is neuroprotective without stimulating erythropoiesis (Gil et al., 2004). Consistent with our study, they found no improvements in motor performance, body weight, or hippocampal neurogenesis. The authors therefore concluded that asialoerythropoietin was not effective in the R6/2 mouse line; however, they did not examine hippocampal atrophy, neurite branching, or spatial cognition, and they may have therefore missed beneficial effects on these HD-related outcomes. Our study was equally limited in the sense that we did not thoroughly characterise all brain regions: we focused on the hippocampus as the lentivirus-induced hEPO expression was enriched in this brain region and because this was the only region in which atrophy was reduced by the LV-hEPO-treatment.

While mouse models of HD have shed light on disease mechanisms, they have not yet led to disease-modifying treatments for human patients. In humans, HD is generally a late-onset neurodegenerative disease, with average onset at approximately 40 years of age (Bates et al., 2015). Disease onset in many HD mouse models is considerably faster than this, which is due to the abnormally high number of CAG repeats in these models and as the mouse life-span is relatively short (approximately 2 years). The R6/2 mouse model also has specific limitations; for example, these mice only express the neurotoxic N-terminal fragment of the mHTT protein (corresponding to exon 1 of the protein) (Mangiarini et al., 1996), which is unlikely to function in precisely the same manner as the full length protein (reviewed in Ehrnhoefer et al., 2009). Regardless of these limitations, our study is one of many to suggest that EPO has therapeutic potential as a neuroprotective agent.

Systemically administered EPO crosses the blood-brain barrier, has neuroprotective and neurotrophic actions, and improves cognition in various neurological and psychiatric disorders (Brines et al., 2000; Agnello et al., 2002; Zhang et al., 2006; Grunfeld et al., 2007; Leconte et al., 2011; Sargin et al., 2010); however, multiple applications of high-dose recombinant EPO are often used to have a therapeutic effect, increasing the risk of EPO-related adverse systemic side-effects. Lentiviral vectors serve as an alternative for gene transfer into the CNS, enabling long-term, stable expression of the desired protein without systemic effects. Using a lentiviral vector, we induced hEPO expression in various regions of the R6/2 brain without altering hematocrit. Although hEPO mRNA and protein were present throughout the brain at the end of the experimental period, we did not explore its expression levels at different time-points during the experimental period. Future studies should characterise the kinetics of gene induction using this gene delivery system, as well its efficacy and safety.

In summary, we present a treatment regime for CNS-restricted EPO expression in HD transgenic mice, which has beneficial effects on HD-related phenotypes while surpassing adverse consequences from long-term systemic applications of EPO. These results may inform future treatment strategies for HD patients and other neurodegenerative diseases.

4. Materials and methods

4.1. Lentiviral vector and viral packing

Lentiviral vectors encoding human erythropoietin (hEPO) were constructed by subcloning hEPO cDNA into the *Cla*I site of pCL20c-MSCV-GFP (Hanawa et al., 2002; Hanawa et al., 2004) and were kindly provided by Dr. Derek Persons (St. Judes Children's Research Hospital, Memphis, TN). The vectors were produced by cotransfection of human embryonic kidney (HEK) 293 T cells with a mixture of four plasmids using the CalPhosTm mammalian transfection kit (Clontech Laboratories, CA, USA). The 293 T cells were cultured in high glucose-containing Dulbecco's modified Eagle's medium (DMEM, Biochrom AG, Berlin, Germany) supplemented with 10% fetal calf serum (Lonza, Vervier, Belgien), 1 mM sodium pyruvate (Sigma-Aldrich, Darmstadt, Germany), 100 U ml^{-1} penicillin and 100 µg/ml streptomycin (Biochrom) at 37 °C and 5% CO2. One day prior to transfection 2.5 × 10^7 293 T cells were plated on 175 cm^2 flasks. The four-plasmid mixture, which consisted of 30 µg pCAGkGP1R, 10 µg pCAG4RTR2, 10 µg pCAG-VSV-G and 50 µg vector plasmid (pCL20c-MSCV), was diluted to a total volume of 2.5 ml with ddH_2O, after which 250 µl of 2 M calcium solution was added. Subsequently, 2.5 ml 2× HBSS was added dropwise while vortexing. The culture medium from each 175 cm^2 flask containing 293 T cells was replaced with 30 ml fresh medium and the DNA-CaPO4 mixture was added dropwise. 18 h after transfection, cells were washed twice with phosphate-buffered saline (PBS) and then 30 ml fresh medium was added. The medium containing the vector particles was harvested 36 h and 54 h after transfection and centrifuged at 500 × *g* for 5 min at 4 °C. The supernatant was passed through a 0.45 µm Filtropur S filter (Sarstedt, Nürnberg, Germany) and the eluent was concentrated using Amicon Ultra centrifugal filters of 50 kDa cut-off (Millipore, Cork, Ireland) at 1500 × g for 60 min at 4 °C. The concentrated virus (~1.2–1.5 ml) was collected from the filter device sample reservoir and ultracentrifuged (90,000 × g, 4 °C, 90 min) using an OptimaTMMax-XP-Ultracentrifuge (Beckmann Coulter GmbH, Krefeld, Germany). The pellet was finally resuspended in 300 µl of 1× PBS, incubated on a rotating platform overnight at 4 °C, aliquoted and stored at −80 °C.

4.2. Lentivirus titration

Titers were determined as infectious units per µl (IFU/µl) by quantitative real-time PCR (qRT-PCR) on genomic DNA of infected primary cortical neurons. Titers were calculated based on standard curves generated form serial dilutions of the pCL20c-MSCV-GFP vector plasmid and cultured primary cortical neurons. In brief, primary cortical neurons were derived from Wistar rat embryos (E17) and cultured using neurobasal medium (NBM) (Gibco) with B27 supplement (Gibco) as previously described by Scheibe et al. (2012). Freshly prepared cortical neurons were seeded into 24-well plates at a density of 325,000 cells/well in a volume of 1 ml NBM per well and were transduced with 1 µl concentrated virus stock. Seven days after transduction, genomic DNA was extracted with a DNeasy blood and tissue kit (Qiagen, Hilden, Germany). The number of IFU/µl was determined by qRT-PCR using the LightCyler Fast Start DNA Master SYBR Green I Kit (Roche, Mannheim, Germany) according to the manufacturer's protocol on a LightCylcer 1.5 (Roche). The following primers were used: MSCV (forward 5′-GGACG TCTCCCAGGGTTGCG-3′ and reverse 5′-GCCCAGCGGTCGTTTTC GTG-3′) and GAPDH (forward 5'-AGATTGTCAGCAATGCATCCTGC-3′, reverse 5′-CCAAGTATGATGACATCAAGAAGG 3′).

4.3. Animals

All mice used in this study were female. Female R6/2 mice (8 weeks of age) expressing exon 1 of the human huntingtin (*HTT*) gene were obtained from the breeding facility of the Charité – Universitätsmedizin. The mice were housed in same sex groups with mixed genotypes. They were placed in a room with controlled temperature and humidity under 12/12 h light/dark cycle and had free access to food and water. The genotype and the number of CAG repeats (146 ± 10) of the mutant *HTT* were determined on ear biopsies by SMB Services (Sequenzierservice ABI BigDye-Terminator-Chemie; Berlin, Germany).

All experimental protocols were approved by the ethics committee of the state of Berlin –Landesamt für Gesundheit und Soziales, LAGeSo, Berlin, Germany (license number: G0143/12). The study was performed in strict accordance with national and international guidelines for the care and use of laboratory animals (Tierschutzgesetz der

Bundesrepublik Deutschland, European directive 2010/63/EU, as well as GV-SOLAS and FELASA guidelines and recommendations for laboratory animal welfare).

4.4. Stereotaxic injection into the subventricular zone (SVZ)

Eight-week-old R6/2 mice were anaesthetised with 2% isoflurane in 70% N_2O, 30% oxygen and maintained during surgery with 1% isofluorane in 70% N_2O, 30% oxygen using a vaporizer (Vapor 19.3, Drägerwerk AG, Lübeck, Germany). Mice were placed in a stereotaxic apparatus (Stoelting, Dublin, Ireland) and after midline incision of the skin, holes slightly bigger than 30 gauges were drilled into the skull. Lentiviral particles produced from either the pCL20c-MSCV-GFP vector or pCL20c-MSCV-hEPO vector (1 μl) at a concentration of 1.3×10^9 IFU/μl were bilaterally injected into cerebroventricles (ICV) at a rate of 0.5 μl/min with a 30-gauge needle on a 5 μl Hamilton syringe. The following coordinates (relative to bregma) were used: 0.4 mm AP, ± 1 mm ML and − 1.5 mm DV according to the stereotaxic atlas of Paxinos and Franklin (Third edition, 2007). After injection, the needle was held in place for an additional 5 min before being slowly removed. Following injection, the incision was sutured, and animals were kept under observation until recovery. To reduce and treat pain, topical lidocaine was used (1%; B. Braun, Melsung, Germany) and buprenophine (0.05 mg/kg) was given via intraperitoneal injections directly after surgery and 12 h following surgery.

4.5. BrdU injections

To evaluate cell proliferation within adult neurogenic niches (i.e. the SVZ and the dentate subgranular zone), mice received six intraperitoneal injections of 50 mg/kg BrdU (Sigma-Aldrich, Darmstadt, Germany) at 12 h intervals starting 1 h after ICV administration of the lentiviral vector.

4.6. Behavioural tests

4.6.1. Y-maze

Spatial working memory of mice was evaluated using a Y-maze by recording spontaneous alternation behaviour in single sessions on day-15 and day-30 after stereotaxic injection. The maze was made of grey plastic and located in a testing room under constant diffuse dim light (35 lx). Each arm was 40 cm long, 10.5 cm high and 3 cm wide. The arms converged in an equilateral triangular central area. The test was performed as described in the literature (Maurice et al., 1994) with slight modifications. Briefly, mice, naïve to the maze, were placed at the end of one arm and allowed to move freely through the maze during an 8 min session. The series of arm entries was recorded visually by a video camera (Panasonic, CCTV camera) positioned above the maze. Arm entry was considered complete when all four limbs of the mouse were entirely within the arm. Alternation was defined as successive entries into the three arms in overlapping triplet sets. Percentage alternation was calculated as the ratio of actual to possible alternations (defined as the total number of arm entries minus one), multiplied by 100. The maze was thoroughly cleaned with 70% ethanol between animals to remove any scent clues left by the previous mouse.

4.6.2. Open field

The total activity in the open field was tested one day before ICV injection and at both 15- and 30-days post-injection, using a VideoMot2 video tracking system (Version 5.68, TSE systems GmbH, Bad Homburg, Germany). The open field was a square arena (50 × 50 cm) with level surface surrounded by 39 cm tall walls. The arena was located in a testing room under constant diffuse dim light (35 lx). Mice were individually placed in the centre of the arena and their exploratory activity in a novel, unfamiliar environment was recorded for 5 min. The total distance travelled by the mice was recorded by a video camera (Panasonic, CCTV camera) positioned above the open field arena. The open field box was thoroughly cleaned with 70% ethanol between animals.

4.6.3. Rotarod

Motor performance of the mice was determined at baseline (one day prior to ICV injection), then 11- and 28-days post-injection using an electrical accelerating rotarod (Process Control RotaRod 3375 series, TSE systems GmbH). The acceleration was set from 4 to 40 RPM over 5 min. The time that the animal was able to stay on the rod was recorded for each performance. Three trials were recorded per mouse with an interval of at least 15 min and the mean was used for statistical analysis.

4.7. Magnetic resonance imaging (MRI)

MRI was performed on mice at baseline (one day prior to ICV injection) and on days 15 and 30 after ICV injection. Mice were anesthetised using 2% isoflurane in 70% N_2O, 30% oxygen. Once fully anaesthetised, mice were positioned and fixed into a plastic frame and were maintained under anaesthesia (1–2% isoflurane) during the scanning. Temperature was maintained through a heat blanket and respiration rate was assessed using a monitoring unit (Small Animal Instruments, SA Instruments, Inc., Stony Brook, USA). Images were acquired on a Bruker 7 T PharmaScan® 70/16 (Bruker Biospin, Ettlingen, Germany) equipped with a 1H-RF quadratur-volume resonator (RAPID Biomedical, Würzburg, Germany) with an inner diameter of 20 mm. The scanner was controlled through Paravision 5.1 software (Bruker). T2*-weighted MRI was achieved with a TurboRARE sequence (imaging parameters: field of view 2.56 × 2.56 cm, slice thickness: 0.5 mm, slice orientation: axial, TE: 36.0 ms, TR: 4200 ms, 32 slices). Twenty axial slices were chosen to cover the region between the olfactory bulb and the cerebellum. To measure mouse brain volumes, T2*-weighted images were processed with ImageJ software (NH, USA) prior to conversion to the Analyze 10 format. Regions of interest (ROIs) were manually delineated onto T2*-weighted images according to Paxinos and Franklin mouse brain atlas (2007) for the hippocampus, striatum, cortex and corpus callosum using Analyze 10.0 (AnalyzeDirect, Overland Park, KS). The region-specific volume was then automatically quantified.

4.8. Hematocrit indices

Mice were anesthetised by subcutaneous injection of a mixture of ketamine (50 mg/kg) and xylazine (7.5 mg/kg). To determine hematocrit indices, blood was drawn from anesthetised mice by periorbital puncture and collected in heparinised hematocrit capillary tubes (Kabe Labortechnik GmbH, Nürnbrecht-Elsenroth, Germany) that were centrifuged in a hematocrit centrifuge (Hettich, Universal 30 RT, Oberhausen, Germany) for 10 min at 1500 x g. Hematocrit was calculated as percentage of packed cell volume of the total blood.

4.9. Immunohistochemistry

Mice were anesthetised by subcutaneous injection of a mixture of ketamine (50 mg/kg) and xylazine (7.5 mg/kg) and transcardially perfused with cold PBS. Brains were dissected, post-fixed in 4% paraformaldehyde (PFA), and subsequently cryoprotected with 30% sucrose in PBS. 40 μm coronal sections of the whole brain were collected using a cryostat.

For BrdU staining, free-floating brain sections were first incubated in 2 N HCL at 37 °C for 30 min and washed in 0.1 M borate buffer (pH 8.5) for 10 min. After washing in 0.1 M Tris-buffered saline (TBS) (pH 7.4), endogenous peroxidase activity was quenched by 0.3% H_2O_2 in TBS for 30 min. After two washes in TBS, sections were blocked at room temperature (RT) for 1 h with 10% goat serum (BIOZOL

Diagnostica, Eching, Germany) in TBS containing 0.3% Triton-X-100 (TBST). The sections were then incubated overnight (4 °C) with anti-BrdU antibody (1:300, Bio-Rad AbD Serotec GmbH, Puchheim, Germany), followed by 2 h incubation with biotinylated secondary antibody (goat-anti-rat IgG, 1:200, Vector Laboratories, CA, USA) at RT. After washing, avidin-biotin-peroxidase complex (Vectastain ABC Elite Kit, Vector Laboratories) was applied for 90 min followed by peroxidase detection for 30 s (0.5 mg/ml 3,3′-diaminobenzidine (Sigma-Aldrich, Darmstadt, Germany) in 0.02% (*v*/v) H_2O_2. Finally, sections were mounted in Roti®-Histokitt (Roth, Karlsruhe, Germany). Doublecortin (DCX), ionised calcium binding adaptor molecule 1 (Iba1) and hEPO were detected according to the above protocol with omission of the HCL incubation and the borate buffer washing step. Primary antibodies were anti-doublecortin (1:400, Santa Cruz, CA, USA), anti-hEPO (1:200, sc-7956, Santa Cruz, CA, USA) and anti-Iba1 (1:500, Wako Chemicals, Neuss, Germany). Biotinylated secondary antibodies were either horse-anti-goat (1:200, Vector Laboratories) or horse-anti-rabbit (1:200, Vector Laboratories).

Immunofluorescence staining for DCX, EPO and NeuN: Briefly, the free-floating sections were blocked with 10% donkey serum in TBST followed by overnight incubation with primary antibodies. After washing, sections were incubated for 4 h at RT with secondary antibodies (Alexa 488- or 594- or 647-IgG, 1:300, Invitrogen, Karlsruhe, Germany). For the Brd-DCX double staining, after the secondary antibody incubation, DCX-stained sections were washed three times in TBS and post-fixed in 4% PFA for 15 min at RT. DNA was denatured in 2 N HCL for 30 min at 37 °C. Sections were post-fixed once more in 4% PFA for 10 min at RT. Following incubation with Proteinase K (0.5 μg/ml) for 4 min at 37 °C, sections were fixed again in 4% PFA for 15 min at RT and washed with TBS. Subsequently, the incubation with anti-BrdU antibody was performed overnight at 4 °C. After washing, sections were incubated with the Alexa 488-IgG secondary antibody for 4 h at RT. Nuclei were counterstained with 4,6-diamidino-2-phenylindole (DAPI) diluted 1:10,000 (Sigma-Aldrich, Darmstadt, Germany). Finally, sections were mounted on slides in FluorSaveTm Reagent (Calbiochem, Bad Soden, Germany).

For immunostaining of huntingtin aggregates and astrocytes, 40 μm free-floating coronal brain sections from WT mice as well as LV-hEPO- and LV-GFP-treated R6/2 mice were used. Sections were first washed with 50 mM TBS for 5 min, then permeabilised with TBST for 10 min at RT, and blocked with 10% NDS (Normal Donkey Serum; Bio-Rad, Neuberg, Germany) in TBST for 1 h at RT. Subsequently, the sections were incubated with the primary antibodies diluted in 1% NDS in TBST overnight at 4 °C on a shaker: rat anti-GFAP (1:1000; Invitrogen) and mouse anti-huntingtin (clone mEM48, 1:200, Millipore). The following day, the tissue was washed three times in TBS at RT, followed by 2 h incubation with the secondary antibodies diluted with 1% NDS in TBST at RT on a shaker: Alexa 568 (1:250, Invitrogen) for EM48 and Alexa 488 (1:250, Invitrogen) for GFAP. The sections were then washed again, incubated with DAPI, and mounted onto slides.

4.10. Imaging and analysis

Double-labelled GFAP/EM48 coronal sections were examined using a confocal laser microscope (Leica SP5 Microsystems) at 200× magnification. For each section, nine images were acquired using the stack imaging tool from the Leica software LAS X in steps of 1 μm, including three images in the cortical area, three in the striatum, and three in the hippocampus. For quantification of the EM48- and GFAP-immunoreactivities, the 3D images were reconstructed and analysed using the Imaris software (Bitplane, Zurich, Switzerland). We created a surface for the channels of EM48 and GFAP immunofluorescence using an automatic surface detail of 0.5 μm for EM48 and 1 μm for GFAP. After manual correction of the absolute intensity threshold (to include only the signal of interest), images were saved and surface volumes for GFAP and EM48 immunofluorescence were compared with total surface volume.

4.11. Cell quantification

In the SVZ, every sixth section (240-μm interval, at the levels relative to bregma 0.14–1.54 mm (Paxinos and Franklin, 2007)) of a hemisphere was analysed on blind-coded slides. Quantification of the target cells in the hippocampal dentate gyrus was conducted on the same number of sections as described for SZV but from 1.8 to 3.3 mm relative to bregma. Cell counting was performed using a light microscope (Leica Microscope DMRA, Wetzlar, Germany) connected to a semi-automatic stereology system (Stereoinvestigator Version 10, MicroBrightField, Magdeburg, Germany). For the quantification of $BrdU^+DCX^+$ cells, all BrdU-labelled cells were analysed for co-expression of DCX using a conventional fluorescence microscope (Leica DM RA2).

4.12. Morphological determination of DCX-positive cells in the DG

The morphological assessment of DCX-positive cells was performed using a light microscope under a 40× oil objective (Leica Microscope DMRA). The number of DCX-positive cells with dendritic morphology and the number of DCX-positive cells that migrate from subgranular zone towards the granule cell layer (GCL) were determined by tracing the borders of the granule cell layer (GCL) adjacent to the molecular cell layer (ML), using a semi-automatic stereology system (MicroBrightField). DCX^+ cells with dendritic branches that did not cross into the ML (immature neuroblasts; Toni and Sultan, 2011) were not counted. For quantification of migrating DCX^+ cells, only cells outside of the subgranular zone were analysed.

4.13. Quantitative real-time PCR

Total RNA of different brain regions was purified using TRIzol (Invitrogen). cDNA synthesis was performed using Superscript II (Invitrogen) following the manufacturer's protocols. Quantitative real-time PCR (qRT-PCR) was performed on a LightCycler 96 (Roche, Mannheim, Germany) using LightCycler FastStar Essential DNA Green Master Kit (Roche) according to the manufacturer's protocol. The following primer pairs were used: hEPO: forward 5′-GGAGGCCGAGAAT ATCACGAC-3′, reverse 5′-CCGTAGAAGTCTGGCAGGG-3′; GFP: forward 5′-CCTGAAGTTCATCTGCACCA-3′, reverse 5′-ACGACGGCAACTACAA GACC-3′; TNF: forward 5′-GACGTGGAACTGGCAGAAGAG-3′, reverse 5′-CCATAGAACTGATGAGAGGGA-3′; CCL2: forward 5′-AGCCAACTCT CACTGAAGCC-3′, reverse 5′-ATCCTCTTGTAGCTCTCCAGCC-3′ and GAPDH: forward 5′-AGATTGTCAGCAATGCATCCTGC-3′, reverse 5′-CCAAGTATGATGACATCA AGAAGG-3′.

4.14. Enzyme-linked immunoassay (ELISA)

Brain samples were homogenised in detergent-free PBS containing complete, EDTA-free protease inhibitor cocktail (Roche, Mannheim, Germany). After 10 min incubation on ice, lysates were centrifuged at 21,000 xg for 20 min at 4 °C. Supernatants were collected and protein concentrations were measured using the BCA™ protein assay kit (Thermo Scientific, Bonn, Germany). The concentration of hEPO was measured using a commercially available ELISA kit (R&D Systems, Abingdon, UK), according to the manufacturer's protocol. The absorbance was determined using a microplate reader (Dynex MRX TC).

4.15. Flow cytometric analysis

Hippocampi were dissected, cut into small pieces and incubated in dissociation buffer (high glucose DMEM containing 5% fetal calf serum (FCS) and 1 mg/ml collagenase (Roche)) at 37 °C for 30 min. The suspension was triturated twice during the incubation period.

Following dissociation, 10 mM of EDTA was added and cells were filtered through a 70 μm cell-strainer. High glucose DMEM was added to a final volume of 30 ml and cells were pelleted at 300 x g for 10 min at 4 °C. Cells were then blocked using anti-CD16/CD32 antibody (Biolegend). The staining of cell surface markers was performed at 4 °C using antibodies against CD45 (FITC, clone 30-F11, Biolegend), CD11b (PerCP-Cy5.5, clone M1/70, BD Biosciences) and MHCII (PE-Cy7, clone M5/114.15.2, Biolegend). Intracellular staining for TNF-α (PE-conjugated, clone TN-3-19/12, BD Biosciences) was performed using the cytofix/cytoperm kit (BD Biosciences). Data were analysed with the FlowJo software (TreeStar).

4.16. Statistical analysis

Quantitative data were shown as independent data points with mean ± SEM. Statistical significance was determined with Prism 6.0 and 8.0 (GraphPad). Normal distribution testing was performed using the Kolmogorov-Smirnov test. Statistical tests used are indicated in respective figure legends. *P* values were considered statistically significant when < 0.05. No randomisation strategy was used in this study. Sample sizes were dependent on the success of our breeding procedure in producing mice with comparable CAG repeat numbers (146 ± 10) and were not predetermined using power calculations. Blinding was performed for the histological analyses, but was not performed for the infections, behavioural assessments, or the MRI assessments. Animals were only excluded from experiments/analyses in cases of mortality and/or humane endpoint.

Funding

This work was supported by grants from the German Research Foundation (FOR1336, SFB/TRR167) and the UK DRI (Momentum Award).

Acknowledgements

We thank Derek Persons†, Gisela Lättig, Francisco Fernández-Klett, and Susanne Mueller for their support. We thank Christian Böttcher and Jasmin Jamal El-Din for technical assistance. The authors declare no competing financial interests.

References

Abordo-Adesida, E., Follenzi, A., Barcia, C., Sciascia, S., Castro, M.G., Naldini, L., Lowenstein, P.R., 2005. Stability of lentiviral vector-mediated transgene expression in the brain in the presence of systemic antivector immune responses. Hum. Gene Ther. 16 (6), 741–751.

Adamcio, B., Sargin, D., Stradomska, A., Medrihan, L., Gertler, C., Theis, F., Zhang, M., Müller, M., Hassouna, I., Hannke, K., Sperling, S., Radyushkin, K., El-Kordi, A., Schulze, L., Ronnenberg, A., Wolf, F., Brose, N., Rhee, J.S., Zhang, W., Ehrenreich, H., 2008. Erythropoietin enhances hippocampal long-term potentiation and memory. BMC Biol. 6, 37.

Agnello, D., Bigini, P., Villa, P., Mennini, T., Cerami, A., Brines, M.L., Ghezzi, P., 2002. Erythropoietin exerts an anti-inflammatory effect on the CNS in a model of experimental autoimmune encephalomyelitis. Brain Res. 952 (1), 128–134.

Almaguer-Melian, W., Mercerón-Martínez, D., Pavón-Fuentes, N., Alberti-Amador, E., Leon-Martinez, R., Ledón, N., Delgado Ocaña, S., Bergado Rosado, J.A., 2015. Erythropoietin promotes neural plasticity and spatial memory recovery in fimbria-fornix-lesioned rats. Neurorehabil. Neural Repair 29 (10), 979–988.

Al-Qahtani, J.M., Abdel-Wahab, B.A., Abd El-Aziz, S.M., 2014. Long-term moderate dose exogenous erythropoietin treatment protects from intermittent hypoxia-induced spatial learning deficits and hippocampal oxidative stress in young rats. Neurochem. Res. 39 (1), 161–171.

Bates, G.P., Dorsey, R., Gusella, J.F., Hayden, M.R., Kay, C., Leavitt, B.R., Nance, M., Ross, C.A., Scahill, R.I., Wetzel, R., Wild, E.J., Tabrizi, S.J., 2015. Huntington disease. Nat Rev Dis Primers. 1, 15005.

Blömer, U., Naldini, L., Kafri, T., Trono, D., Verma, I.M., Gage, F.H., 1997. Highly efficient and sustained gene transfer in adult neurons with a lentivirus vector. J. Virol. 71 (9), 6641–6649.

Bradford, J., Shin, J.Y., Roberts, M., Wang, C.E., Li, X.J., Li, S., 2009. Expression of mutant huntingtin in mouse brain astrocytes causes age-dependent neurological symptoms. Proc. Natl. Acad. Sci. U. S. A. 106 (52), 22480–22485.

Brines, M.L., Ghezzi, P., Keenan, S., Agnello, D., de Lanerolle, N.C., Cerami, C., Itri, L.M., Cerami, A., 2000. Erythropoietin crosses the blood-brain barrier to protect against experimental brain injury. Proc. Natl. Acad. Sci. U. S. A. 97 (19), 10526–10531.

Bulley, S.J., Drew, C.J., Morton, A.J., 2012. Direct visualisation of abnormal dendritic spine morphology in the hippocampus of the R6/2 transgenic mouse model of Huntington's disease. J. Huntingtons Dis. 1 (2), 267–273.

Carter, R.J., Lione, L.A., Humby, T., Mangiarini, L., Mahal, A., Bates, G.P., Dunnett, S.B., Morton, A.J., 1999. Characterization of progressive motor deficits in mice transgenic for the human Huntington's disease mutation. J. Neurosci. 19 (8), 3248–3257.

Chen, Z.Y., Asavaritikrai, P., Prchal, J.T., Noguchi, C.T., 2007. Endogenous erythropoietin signaling is required for normal neural progenitor cell proliferation. J. Biol. Chem. 282 (35), 25875–25883.

Czéh, B., Lucassen, P.J., 2007. What causes the hippocampal volume decrease in depression? Are neurogenesis, glial changes and apoptosis implicated? Eur. Arch. Psychiatry Clin. Neurosci. 257 (5), 250–260.

DiFiglia, M., Sapp, E., Chase, K.O., Davies, S.W., Bates, G.P., Vonsattel, J.P., Aronin, N., 1997. Aggregation of huntingtin in neuronal intranuclear inclusions and dystrophic neurites in brain. Science. 277 (5334), 1990–1993.

Digicaylioglu, M., Bichet, S., Marti, H.H., Wenger, R.H., Rivas, L.A., Bauer, C., Gassmann, M., 1995. Localization of specific erythropoietin binding sites in defined areas of the mouse brain. Proc. Natl. Acad. Sci. U. S. A. 92 (9), 3717–3720.

Ehrenreich, H., Aust, C., Krampe, H., Jahn, H., Jacob, S., Herrmann, M., Sirén, A.L., 2004. Erythropoietin: novel approaches to neuroprotection in human brain disease. Metab. Brain Dis. 19 (3–4), 195–206.

Ehrenreich, H., Fischer, B., Norra, C., Schellenberger, F., Stender, N., Stiefel, M., Sirén, A.L., Paulus, W., Nave, K.A., Gold, R., Bartels, C., 2007. Exploring recombinant human erythropoietin in chronic progressive multiple sclerosis. Brain. 130 (Pt 10), 2577–2588.

Ehrnhoefer, D.E., Butland, S.L., Pouladi, M.A., Hayden, M.R., 2009. Mouse models of Huntington disease: variations on a theme. Dis. Model. Mech. 2 (3–4), 123–129.

El-Akabawy, G., Rattray, I., Johansson, S.M., Gale, R., Bates, G., Modo, M., 2012. Implantation of undifferentiated and pre-differentiated human neural stem cells in the R6/2 transgenic mouse model of Huntington's disease. BMC Neurosci. 13, 97.

Ellrichmann, G., Blusch, A., Fatoba, O., Brunner, J., Hayardeny, L., Hayden, M., Sehr, D., Winklhofer, K.F., Saft, C., Gold, R., 2017. Laquinimod treatment in the R6/2 mouse model. Sci. Rep. 7 (1), 4947.

Fassler, M., Weissberg, I., Levy, N., Diaz-Griffero, F., Monsonego, A., Friedman, A., Taube, R., 2013. Preferential lentiviral targeting of astrocytes in the central nervous system. PLoS One 8 (10), e76092.

Genc, S., Akhisaroglu, M., Kuralay, F., Genc, K., 2002. Erythropoietin restores glutathione peroxidase activity in 1-methyl-4-phenyl-1,2,5,6-tetrahydropyridine-induced neurotoxicity in C57BL mice and stimulates murine astroglial glutathione peroxidase production in vitro. Neurosci. Lett. 321 (1–2), 73–76.

Gil, J.M., Leist, M., Popovic, N., Brundin, P., Petersén, A., 2004. Asialoerythropoietin is not effective in the R6/2 line of Huntington's disease mice. BMC Neurosci. 5, 17.

Girgenti, M.J., Hunsberger, J., Duman, C.H., Sathyanesan, M., Terwilliger, R., Newton, S.S., 2009. Erythropoietin induction by electroconvulsive seizure, gene regulation, and antidepressant-like behavioral effects. Biol. Psychiatry 66 (3), 267–274.

Grunfeld, J.F., Barhum, Y., Blondheim, N., Rabey, J.M., Melamed, E., Offen, D., 2007. Erythropoietin delays disease onset in an amyotrophic lateral sclerosis model. Exp. Neurol. 204 (1), 260–263.

Hageman, I., Nielsen, M., Wortwein, G., Diemer, N.H., Jorgensen, M.B., 2008. Electroconvulsive stimulations prevent stress-induced morphological changes in the hippocampus. Stress. 11 (4), 282–289.

Hanawa, H., Kelly, P.F., Nathwani, A.C., Persons, D.A., Vandergriff, J.A., Hargrove, P., Vanin, E.F., Nienhuis, A.W., 2002. Comparison of various envelope proteins for their ability to pseudotype lentiviral vectors and transduce primitive hematopoietic cells from human blood. Mol. Ther. 5 (3), 242–251.

Hanawa, H., Hargrove, P.W., Kepes, S., Srivastava, D.K., Nienhuis, A.W., Persons, D.A., 2004. Extended beta-globin locus control region elements promote consistent therapeutic expression of a gamma-globin lentiviral vector in murine beta-thalassemia. Blood. 104 (8), 2281–2290.

Hockly, E., Cordery, P.M., Woodman, B., Mahal, A., van Dellen, A., Blakemore, C., Lewis, C.M., Hannan, A.J., Bates, G.P., 2002. Environmental enrichment slows disease progression in R6/2 Huntington's disease mice. Ann. Neurol. 51 (2), 235–242.

Huntington's Disease Collaborative Research Group, 1993. A novel gene containing a trinucleotide repeat that is expanded and unstable on Huntington's disease chromosomes. Cell. 72 (6), 971–983.

Jakobsson, J., Ericson, C., Jansson, M., Björk, E., Lundberg, C., 2003. Targeted transgene expression in rat brain using lentiviral vectors. J. Neurosci. Res. 73 (6), 876–885.

Kantor, B., McCown, T., Leone, P., Gray, S.J., 2014. Clinical applications involving CNS gene transfer. Adv. Genet. 87, 71–124.

Kumral, A., Tugyan, K., Gonenc, S., Genc, K., Genc, S., Sonmez, U., Yilmaz, O., Duman, N., Uysal, N., Ozkan, H., 2005. Protective effects of erythropoietin against ethanol-induced apoptotic neurodegenaration and oxidative stress in the developing C57BL/6 mouse brain. Brain Res. Dev. Brain Res. 160 (2), 146–156.

Leconte, C., Bihel, E., Lepelletier, F.X., Bouët, V., Saulnier, R., Petit, E., Boulouard, M., Bernaudin, M., Schumann-Bard, P., 2011. Comparison of the effects of erythropoietin and its carbamylated derivative on behaviour and hippocampal neurogenesis in mice. Neuropharmacology. 60 (2–3), 354–364.

Li, J.Y., Popovic, N., Brundin, P., 2005. The use of the R6 transgenic mouse models of Huntington's disease in attempts to develop novel therapeutic strategies. NeuroRx. 2 (3), 447–464.

Lu, D., Mahmood, A., Qu, C., Goussev, A., Schallert, T., Chopp, M., 2005. Erythropoietin enhances neurogenesis and restores spatial memory in rats after traumatic brain injury. J. Neurotrauma 22 (9), 1011–1017.

Mangiarini, L., Sathasivam, K., Seller, M., Cozens, B., Harper, A., Hetherington, C., Lawton, M., Trottier, Y., Lehrach, H., Davies, S.W., Bates, G.P., 1996. Exon 1 of the HD gene with an expanded CAG repeat is sufficient to cause a progressive neurological phenotype in transgenic mice. Cell. 87 (3), 493–506.

Maurice, T., Hiramatsu, M., Itoh, J., Kameyama, T., Hasegawa, T., Nabeshima, T., 1994. Behavioral evidence for a modulating role of sigma ligands in memory processes. I. Attenuation of dizocilpine (MK-801)-induced amnesia. Brain Res. 647 (1), 44–56.

McIver, S.R., Lee, C.S., Lee, J.M., Green, S.H., Sands, M.S., Snider, B.J., Goldberg, M.P., 2005. Lentiviral transduction of murine oligodendrocytes in vivo. J. Neurosci. Res. 82 (3), 397–403.

Miskowiak, K.W., Vinberg, M., Macoveanu, J., Ehrenreich, H., Køster, N., Inkster, B., Paulson, O.B., Kessing, L.V., Skimminge, A., Siebner, H.R., 2015. Effects of erythropoietin on hippocampal volume and memory in mood disorders. Biol. Psychiatry 78 (4), 270–277.

Morozko, E.L., Ochaba, J., Hernandez, S.J., Lau, A., Sanchez, I., Orellana, I., Kopan, L., Crapser, J., Duong, J.H., Overman, J., Yeung, S., Steffan, J.S., Reidling, J., Thompson, L.M., 2018. Longitudinal biochemical assay analysis of mutant huntingtin exon 1 protein in R6/2 mice. J. Huntingtons Dis. 7 (4), 321–335.

Murphy, K.P., Carter, R.J., Lione, L.A., Mangiarini, L., Mahal, A., Bates, G.P., Dunnett, S.B., Morton, A.J., 2000. Abnormal synaptic plasticity and impaired spatial cognition in mice transgenic for exon 1 of the human Huntington's disease mutation. J. Neurosci. 20 (13), 5115–5123.

Oh, D.H., Lee, I.Y., Choi, M., Kim, S.H., Son, H., 2012. Comparison of neurite outgrowth induced by erythropoietin (EPO) and carbamylated erythropoietin (CEPO) in hippocampal neural progenitor cells. Korean J. Physiol. Pharmacol. 16 (4), 281–285.

O'Keefe, J., Nadel, L., 1978. The Hippocampus as a Cognitive Map. Oxford University Press.

Othman, M.A.M., Rajab, E., AlMubarak, A., AlNaisar, M., Bahzad, N., Kamal, A., 2018. Erythropoietin protects against cognitive impairment and hippocampal neurodegeneration in diabetic mice. Behav. Sci. (Basel) 9 (1) Pii: E4.

Patel, N.S., Nandra, K.K., Thiemermann, C., 2012. Bench-to-bedside review: erythropoietin and its derivatives as therapies in critical care. Crit. Care 16 (4), 229.

Paxinos, G., Franklin, K.B.J., 2007. The Mouse Brain in Stereotaxic Coordinates, Third edition. .

Peng, Q., Masuda, N., Jiang, M., Li, Q., Zhao, M., Ross, C.A., Duan, W., 2008. The antidepressant sertraline improves the phenotype, promotes neurogenesis and increases BDNF levels in the R6/2 Huntington's disease mouse model. Exp. Neurol. 210 (1), 154–163.

Phillips, W., Morton, A.J., Barker, R.A., 2005. Abnormalities of neurogenesis in the R6/2 mouse model of Huntington's disease are attributable to the in vivo microenvironment. J. Neurosci. 25 (50), 11564–11576.

Ross, C.A., Tabrizi, S.J., 2011. Huntington's disease: from molecular pathogenesis to clinical treatment. Lancet Neurol. 10 (1), 83–98.

Sargin, D., Friedrichs, H., El-Kordi, A., Ehrenreich, H., 2010. Erythropoietin as neuroprotective and neuroregenerative treatment strategy: comprehensive overview of 12 years of preclinical and clinical research. Best Pract. Res. Clin. Anaesthesiol. 24 (4), 573–594.

Sathyanesan, M., Watt, M.J., Haiar, J.M., Scholl, J.L., Davies, S.R., Paulsen, R.T., Wiederin, J., Ciborowski, P., Newton, S.S., 2018. Carbamoylated erythropoietin modulates cognitive outcomes of social defeat and differentially regulates gene expression in the dorsal and ventral hippocampus. Transl. Psychiatry 8 (1), 113.

Scheibe, F., Klein, O., Klose, J., Priller, J., 2012. Mesenchymal stromal cells rescue cortical neurons from apoptotic cell death in an in vitro model of cerebral ischemia. Cell. Mol. Neurobiol. 32 (4), 567–576.

Schiefer, J., Alberty, A., Dose, T., Oliva, S., Noth, J., Kosinski, C.M., 2002. Huntington's disease transgenic mice are resistant to global cerebral ischemia. Neurosci. Lett. 334 (2), 99–102.

Schmidt-Hieber, C., Nolan, M.F., 2017. Synaptic integrative mechanisms for spatial cognition. Nat. Neurosci. 20 (11), 1483–1492.

Shingo, T., Sorokan, S.T., Shimazaki, T., Weiss, S., 2001. Erythropoietin regulates the in vitro and in vivo production of neuronal progenitors by mammalian forebrain neural stem cells. J. Neurosci. 21 (24), 9733–9743.

Simmons, D.A., James, M.L., Belichenko, N.P., Semaan, S., Condon, C., Kuan, J., Shuhendler, A.J., Miao, Z., Chin, F.T., Longo, F.M., 2018. TSPO-PET imaging using [18F]PBR06 is a potential translatable biomarker for treatment response in Huntington's disease: preclinical evidence with the p75NTR ligand LM11A-31. Hum. Mol. Genet. 27 (16), 2893–2912.

Spargo, E., Everall, I.P., Lantos, P.L., 1993. Neuronal loss in the hippocampus in Huntington's disease: a comparison with HIV infection. J. Neurol. Neurosurg. Psychiatry 56 (5), 487–491.

Squitieri, F., Di Pardo, A., Favellato, M., Amico, E., Maglione, V., Frati, L., 2015. Pridopidine, a dopamine stabilizer, improves motor performance and shows neuroprotective effects in Huntington disease R6/2 mouse model. J. Cell. Mol. Med. 19 (11), 2540–2548.

Stack, E.C., Kubilus, J.K., Smith, K., Cormier, K., Del Signore, S.J., Guelin, E., Ryu, H., Hersch, S.M., Ferrante, R.J., 2005. Chronology of behavioral symptoms and neuropathological sequela in R6/2 Huntington's disease transgenic mice. J. Comp. Neurol. 490 (4), 354–370.

Stack, E.C., Smith, K.M., Ryu, H., Cormier, K., Chen, M., Hagerty, S.W., Del Signore, S.J., Cudkowicz, M.E., Friedlander, R.M., Ferrante, R.J., 2006. Combination therapy using minocycline and coenzyme Q10 in R6/2 transgenic Huntington's disease mice. Biochim. Biophys. Acta 1762 (3), 373–380.

Toni, N., Sultan, S., 2011. Synapse formation on adult-born hippocampal neurons. Eur. J. Neurosci. 33 (6), 1062–1068.

Wang, L., Zhang, Z.G., Zhang, R.L., Jiao, Z.X., Wang, Y., Pourabdollah-Nejad, D.S., LeTourneau, Y., Gregg, S.R., Chopp, M., 2006. Neurogenin 1 mediates erythropoietin enhanced differentiation of adult neural progenitor cells. J. Cereb. Blood Flow Metab. 26 (4), 556–564.

Wen, T.C., Sadamoto, Y., Tanaka, J., Zhu, P.X., Nakata, K., Ma, Y.J., Hata, R., Sakanaka, M., 2002. Erythropoietin protects neurons against chemical hypoxia and cerebral ischemic injury by up-regulating Bcl-xL expression. J. Neurosci. Res. 67 (6), 795–803.

Wüstenberg, T., Begemann, M., Bartels, C., Gefeller, O., Stawicki, S., Hinze-Selch, D., Mohr, A., Falkai, P., Aldenhoff, J.B., Knauth, M., Nave, K.A., Ehrenreich, H., 2011. Recombinant human erythropoietin delays loss of gray matter in chronic schizophrenia. Mol. Psychiatry 16 (1), 26–36.

Zhang, F., Signore, A.P., Zhou, Z., Wang, S., Cao, G., Chen, J., 2006. Erythropoietin protects CA1 neurons against global cerebral ischemia in rat: potential signaling mechanisms. J. Neurosci. Res. 83 (7), 1241–1251.

Zhang, F., Wang, S., Cao, G., Gao, Y., Chen, J., 2007. Signal transducers and activators of transcription 5 contributes to erythropoietin-mediated neuroprotection against hippocampal neuronal death after transient global cerebral ischemia. Neurobiol. Dis. 25 (1), 45–53.